Effect of channel width on the primary instability of inclined film flow

M. Vlachogiannis,[1,2] A. Samandas,[1] V. Leontidis,[1] and V. Bontozoglou[1]
[1]*Department of Mechanical Engineering, University of Thessaly, GR-38334 Volos, Greece*
[2]*Technological Educational Institute of Larissa, GR-41110 Larissa, Greece*

(Received 24 May 2009; accepted 30 November 2009; published online 26 January 2010)

A procedure is developed to detect the onset of interfacial instability in inclined film flows (with estimated accuracy better than 5%) and is used to show that the finite width of experimental channels stabilizes the undisturbed liquid film. Deviation from the classical prediction scales inversely with the product of channel width and sine of inclination angle, and for small inclinations and/or narrow channels is of the order of 100%. The effect is tentatively attributed to the influence of sidewalls on the traveling disturbances, which results in curved crestlines and transverse variation of wave characteristics. © *2010 American Institute of Physics*. [doi:10.1063/1.3294884]

I. INTRODUCTION

It is well-known that film flows at all inclinations beyond a few tenths of a degree are first destabilized by an interfacial mode, whose streamwise scale is significantly larger than the mean film thickness.[1–4] A long-wave expansion, based on this observation and exploiting Squire's theorem for streamwise disturbances, leads to the classical result[5,6] that the critical Reynolds number for the onset of primary instability depends only on inclination angle θ, according to the relation

$$\mathrm{Re}_c = \tfrac{5}{6}\cot\theta, \tag{1}$$

where Re is defined as $\mathrm{Re}=\mathrm{hu}/\nu$ in terms of kinematic viscosity ν, undisturbed film thickness h, and mean liquid velocity u. The mechanism of instability is associated with a balance between rate of work done by the perturbation shear stress at the surface and rate of viscous dissipation in the bulk.[3,4] Because the most unstable disturbances are very long, surface tension plays no role in the initial growth stage. However, surface tension determines the characteristics of the coherent structures (solitary waves) that develop in the nonlinear regime by balancing the gravity-induced inertia of the liquid humps with the capillary force that arises from the wrinkling of the surface into a series of precursor ripples.[7]

Verification of the accuracy of the linear prediction, Eq. (1), met with significant difficulties, because disturbance growth near the stability threshold is too weak to permit direct observation.[8] For example, a vertical film may appear flat for Reynolds numbers as high as 3–5. A more reliable criterion is provided by measuring the growth/decay of regular small amplitude disturbances introduced at the inlet. The decisive experiment was done by Liu *et al.*[9] using disturbances of controlled frequency f in a channel 500 mm wide. According to the authors, the procedure is very tedious and its accuracy is estimated as no better than 10%.

The present paper investigates experimentally the dependence of linear stability of film flow on the width of the channel. The conclusions are relevant to experiments performed along planar substrates bounded by sidewalls, which have actually provided the majority of available results in the literature. However, it is noted that, in the case of a vertical film, use of a cylinder with radius much larger than the Nusselt film thickness would give results asymptotically equivalent to a flat substrate but without the complications of the sidewalls.

More specifically, in the present context of a planar substrate, the finite width of experimental channels poses the question of the significance of edge effects. This question has two facets: one is the effect of the sidewalls on the base flow with undisturbed free surface and the other is the effect of the sidewalls on the form and evolution of traveling disturbances. The former question was already posed in classical literature[10] but was comprehensively answered only recently.[11] The latter question appears not to have been discussed at all and provides the theme of the present paper.

Concerning the unidirectional base flow with undisturbed free surface, a first approximation may be made by neglecting wetting effects or equivalently, assuming a 90° contact angle at the sidewalls. Then, film flow is formally identical to the flow inside a rectangular channel with height equal to twice the film thickness. The available analytic solution to this problem by separation of variables[12] indicates that the key parameter is the ratio of film thickness to channel width, $\mathrm{k}=\mathrm{h}/\mathrm{w}$, which in experiments is typically in the range of 10^{-2}–10^{-3}. For small values of this ratio, the influence of sidewalls is limited to a transverse distance of the order of the film thickness, and the major part of the base flow may safely be considered as one-dimensional. When wetting effects are considered, the normal capillary length scale, $\mathrm{L_n}=(\sigma/\rho g\cos\theta)^{1/2}$—defined by a balance of surface tension and gravity component normal to the wall—comes into play, and an interesting overshoot in the free surface velocity close to the wall may appear when the ratio $\mathrm{L_n}/\mathrm{h}$ exceeds order one.[11] However, for the typical experimental scaling $\mathrm{L_n}\ll\mathrm{w}$, the influence of sidewalls is again limited to a small region in their vicinity and the bulk of the base flow conforms to the Nusselt solution.

Though it may safely be concluded from the above that sidewall effects are insignificant for the undisturbed film flow in typical experimental realizations, there are strong indications that this is not the case when the flow becomes unstable. More specifically, it has been repeatedly observed that the crestlines of traveling disturbances become sym-

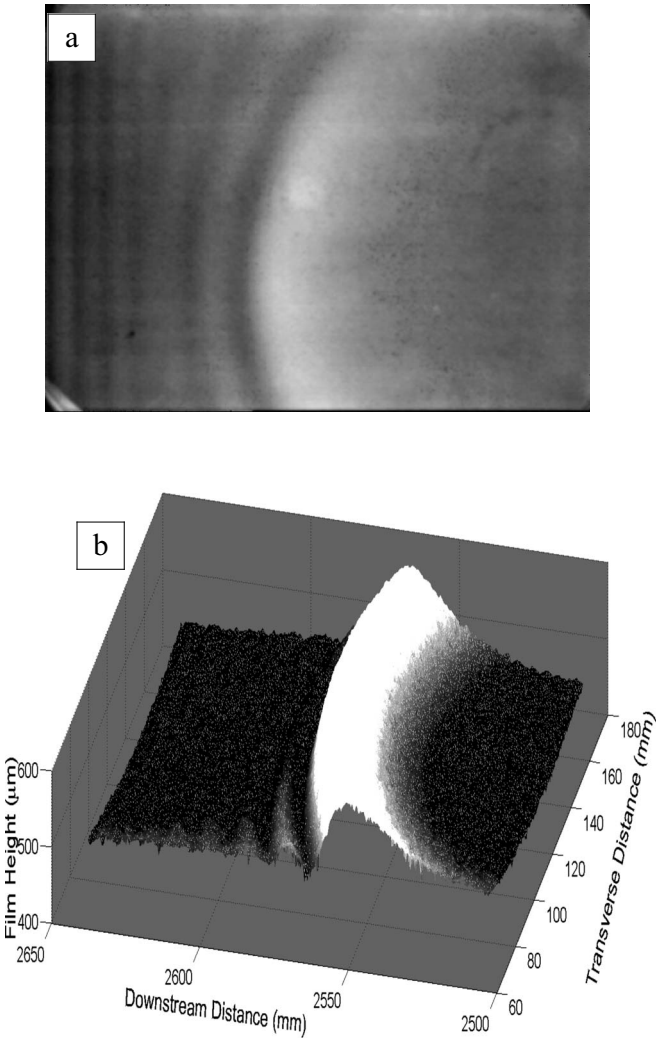

FIG. 1. (a) Gray scale image (with brightness proportional to the local film thickness) of a traveling wave with symmetrically curved crestlines. (b) The same wave in a 3D plot. The liquid is water at Re=30, φ=5°, and f =1.0 Hz.

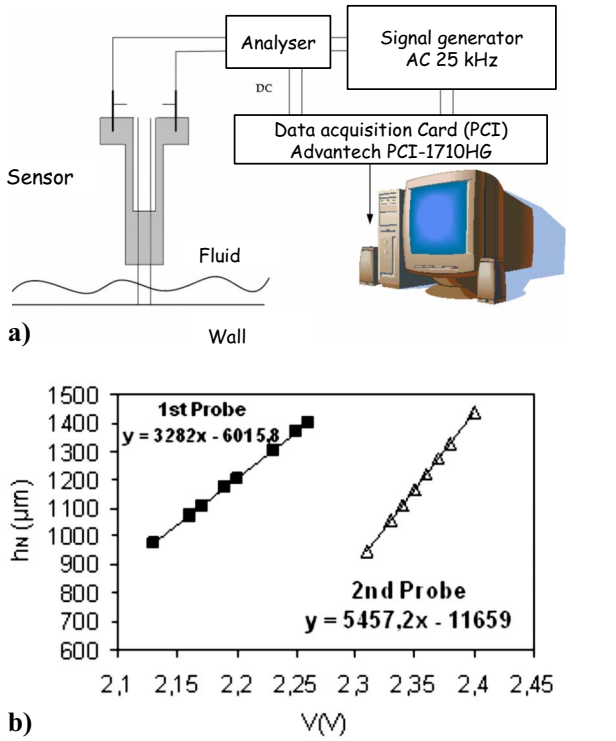

FIG. 2. (Color online) (a) A sketch of the experimental setup for the implementation of the conductivity technique. (b) The output voltage as a function of the Nusselt film thickness for inclination angle φ=25° and 76% glycerol aqueous solution.

metrically curved around the channel centerplane.[13,14] This behavior is depicted in Fig. 1. Figure 1(a) is a gray scale image of a traveling wave taken from below the channel, where brightness is proportional to local film thickness. Figure 1(b) is a three-dimensional (3D) plot of the same wave. Intuitively, the curved crestline may only be attributed to an effect of the sidewalls that evidently extends throughout the channel width. Measurements taken at the central strip of the channel have been assumed representative of the theoretical limit of two-dimensional (2D) flow,[9,15] based on the argument that the ratio k of film thickness to channel width is very small. However, there exist consistent discrepancies between solitary wave heights measured and predicted by rigorous simulations,[16–19] and the curvature of the crestlines was recently proposed as a tentative cause.[20]

The present work reports systematic measurements of the linear stability threshold in inclined film flows as a function of channel width. Section II describes the experimental system and the measuring technique. Section III presents the results: a procedure is developed to identify the transition, which appears to be less tedious and slightly more accurate than the previous one in the literature. The data indicate that liquid films at small and intermediate inclination angles are significantly more stable than predicted by the classical result with the discrepancy aggravating with decreasing channel inclination and width. A mechanistic interpretation of the effect of sidewalls is proposed, related to the crestline curvature and the variation of wave characteristics in the transverse direction. This conjecture is further discussed in the concluding remarks of Sec. IV and provides motivation for a detailed study of the characteristics of curved, traveling waves observed beyond the primary transition.

II. EXPERIMENTAL METHOD

The main flow facility is an 800 mm long by 250 mm wide channel made of Plexiglas. The width of the channel can be restricted by placing along the sidewalls of two Plexiglas plates of appropriate size. Using this technique, measurements are taken for active channel widths 250, 166, and 83 mm. Representative results are also confirmed in a newly built inclined film facility, 3000 mm long and up to 450 mm wide. The liquids used in the experiments are water-glycerol solutions with 30–80 wt % in glycerol, maintained at a temperature of 25 ± 1 °C. The inclination angles tested cover the range of 5°–30°. With increasing inclination, the glycerol content also increases so that the liquid film always remains thick enough to avoid rupture. Few experiments are done after saturation of the glycerol aqueous solution with butanol (~7%), which leads to a drastic decrease in surface tension.

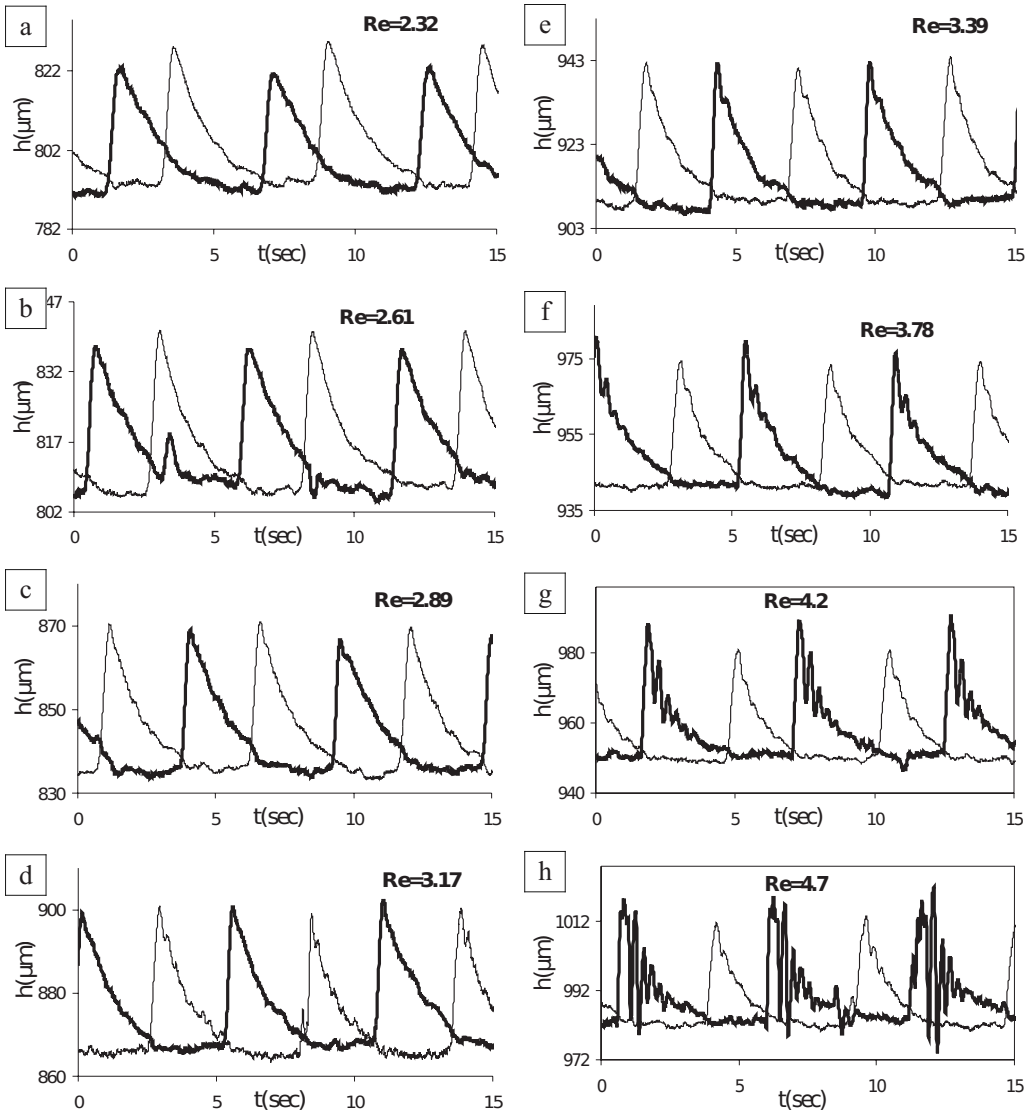

FIG. 3. Time series of liquid film height for a 66 wt % glycerol in water solution at various Reynolds numbers around the primary transition. Channel inclination and width are, respectively, $\varphi=15°$, w=166 mm, and inlet disturbances have frequency f=0.167 Hz. Here and in all subsequent plots, we represent by thin lines, the upstream and by thick lines, the downstream signal.

A system of perturbing the entrance flow rate at desired frequency is used, based on the periodic obstruction of a by-pass liquid stream. The obstruction is imposed either abruptly by an electrovalve, resulting in a steep-crested disturbance or more smoothly through modulation of a control valve; thus resulting in a roughly sinusoidal disturbance. The frequencies used span in the range of 0.167–1.50 Hz and all result in disturbances that are very long when compared with the liquid film thickness.

The spatial evolution of traveling disturbances is determined by comparing time signals of the free surface height taken by conductance probes at streamwise locations 150 and 650 mm from the film entrance. Each probe, sketched in Fig. 2(a), consists of two parallel chromel wires, 0.4 mm in diameter, separated by an axis-to-axis distance of 2 mm. A function generator provides an input sinusoidal signal to the probes at a frequency of 25 000 Hz in order to avoid polarization effects. The output signal is a sinusoidal voltage whose amplitude depends linearly on system conductance and thus varies with the coverage of the wires by the liquid. The probes are simultaneously calibrated *in situ* by taking measurements of the output voltage in the stable flow regime (without inlet disturbances) and calculating the film thickness from the Nusselt solution. The output voltage of both probes varies linearly with the Nusselt film thickness as it is depicted for a representative case in Fig. 2(b).

III. RESULTS

A. Determination of marginal stability

A secondary goal of the present paper is to develop an experimental method to detect the primary transition, which is reliable but at the same time less tedious than the method previously used.[9,21] We recall that the standard approach of these authors is based on measurement by laser beam deflection of the wave slope at two different locations along the flow. For a given Reynolds number—above the expected critical—disturbances of varying frequency are consecu-

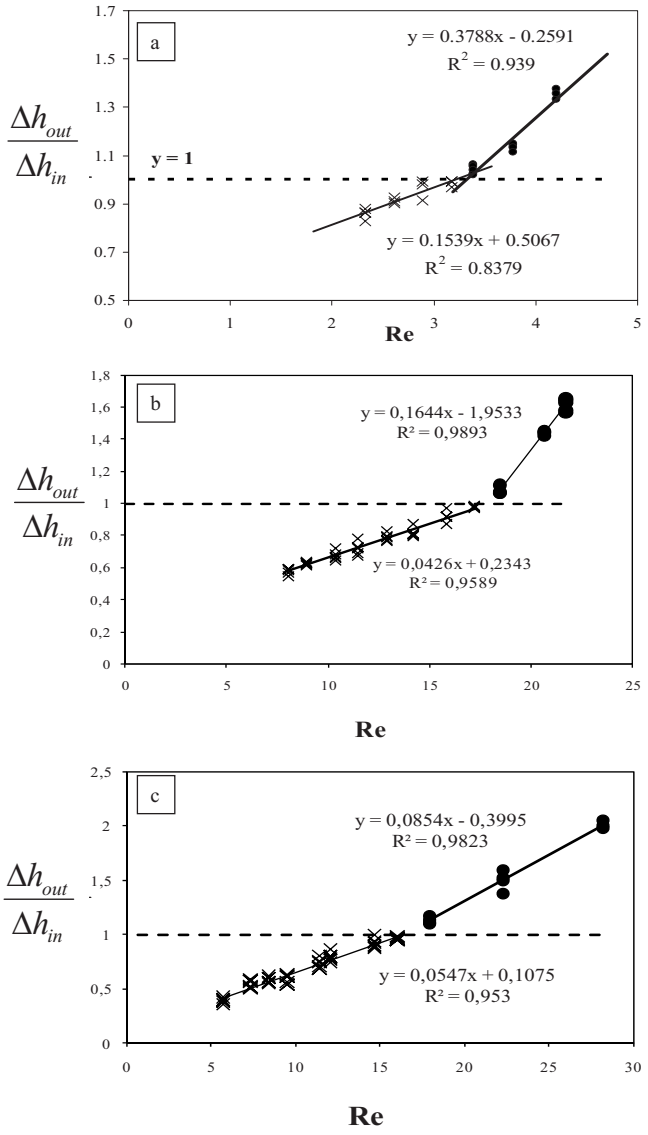

FIG. 4. Determination of marginal stability for: (a) inclination angle $\varphi=15°$ and channel width w=166 mm. (b) $\varphi=5°$ and w=166 mm. (c) $\varphi=5°$ and w=250 mm.

tively introduced and the cutoff frequency is determined, beyond which the spectral power of the time series of the wave slope declines from the first to the second measuring location. This procedure is repeated for sufficiently many Re's to permit interpolation to the zero frequency limit according to the theoretically expected behavior of $f_c \sim (\mathrm{Re}-\mathrm{Re}_c)^{1/2}$.

Our approach is more direct. It relies on the introduction of disturbances of very low frequency (typically f=0.167 Hz), such that the critical Re of linear stability practically coincides with that of the theoretical disturbance of zero frequency (infinite wavelength). The downstream development of such low-frequency disturbances is qualitatively different in the stable and unstable regimes. This difference provides added confidence to the quantitative determination, which involves comparison of the wave height at the two observing locations, as a function of the Reynolds number.

A typical example of film height time series is shown in Fig. 3, corresponding to inclination angle $\varphi=15°$, channel

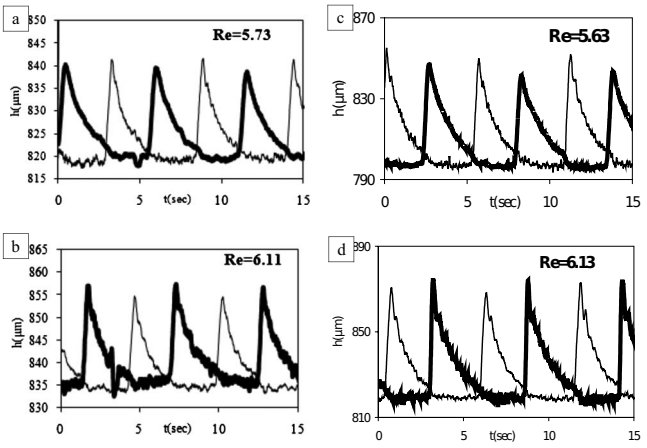

FIG. 5. Time series at Re values bracketing the transition for two realizations at inclination angle $\varphi=10°$ and channel width w=166 mm. Disturbances have frequency f=0.167 Hz in both cases, but height around 20 μm in the first [(a) and (b)] and 50 μm in the second [(c) and (d)].

width w=166 mm, and inlet frequency f=0.167 Hz. In all figures, thin lines always represent the upstream and thick lines the downstream signal. The two signals are compared for eight values of Re, the first four residing in the stable regime and the last four in the unstable. For the stable Re values, the wave height at the second location is always lower than at the first and the overall shape of the wave remains unaltered. For the unstable Re values, the wave height at the second location grows beyond that at the first, but—more important—the wave shape changes drastically, disintegrating into a series of shorter waves. This easily detectable change in wave evolution with increasing Re brackets the range where the transition takes place, and serves as a check of the quantitative determination that follows. Thus, in the present example it may be inferred that the stability limit lies in the range of $3.17<\mathrm{Re}<3.78$.

The quantitative determination of marginal stability is depicted in Fig. 4 for three representative cases, corresponding to different channel inclinations and widths. It is based on the observation of the parametric evolution with Re of the ratio of downstream to upstream wave height. To improve measurement accuracy, the wave heights are normalized with the measured mean film thickness at the respective probe locations. Two characteristics facilitate reliable determination of the transition. First, the ratio is lower than one in the stable and higher than one in the unstable regime. Second, its rate of change with Re exhibits a jump when crossing the stability limit. Thus, we identify the critical Re with the coincidence of three lines: one is the horizontal corresponding to ratio=1 and the other two are linear interpolations of the last (first) few points before (after) the transition. Of the two linear interpolations, the former (points before transition) typically exhibits a higher scatter and is neglected in case the three lines do not cross at exactly the same point.

Before embarking into the main result of the paper, which is the stabilizing effect of channel width, it is necessary to confirm the absence of effect of the disturbance amplitude, frequency, and shape, i.e., verify that the disturbances used are linear and long enough, and that the specific

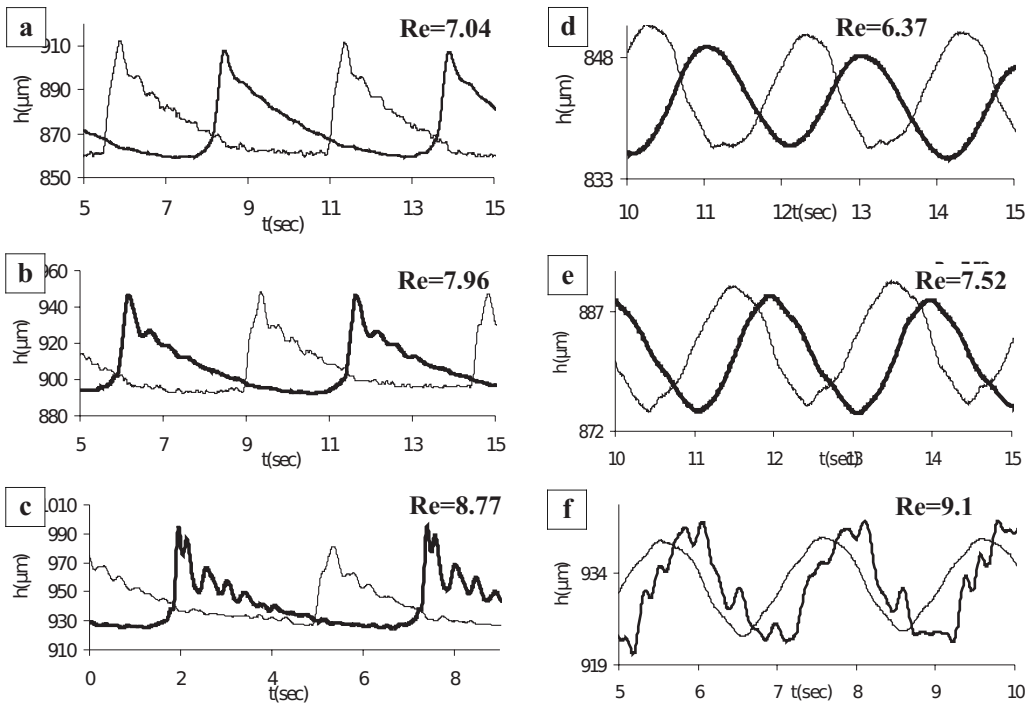

FIG. 6. Time series at Re values bracketing the transition for two experiments at inclination angle $\varphi=10°$ and channel width w=83 mm. Inlet disturbances are steep-crested in the first one [(a)–(c)] and sinusoidal in the second [(d)–(f)].

form chosen does not bias the results. With respect to the effect of amplitude, we note that typical inlet disturbances have a height around 5% of the mean film thickness and that duplicate experiments with disturbance height as low as 1%–2% result in identical critical Re. As an example, the time series at Re values bracketing the instability threshold are shown in Fig. 5 for two realizations of a representative case ($\varphi=10°$, w=166 mm, and f=0.167 Hz). Disturbances have frequency f=0.167 Hz in both cases, but height around 20 μm in the first [Figs. 5(a) and 5(b)] and 50 μm in the second [Figs. 5(c) and 5(d)].

With respect to the shape of the inlet disturbance, we note that experiments are typically done with steep-crested disturbances but many have been duplicated with disturbances of sinusoidal shape and the critical Re was always indistinguishable within experimental error. As an example, Fig. 6 compares the respective time series for inclination $\varphi=10°$ and channel width w=83 mm, and shows that the same qualitative change in wave shape (i.e., the disintegration into a series of shorter waves) is observed with both types of disturbance. Quantitative determination of the stability threshold for the two cases in Fig. 6, produced the values 8.0 and 8.1, respectively.

Concerning the effect of the frequency of inlet disturbances, we want to confirm that the typically used value, f=0.167 Hz, is low enough for the experimentally determined critical Re to coincide with the respective value for disturbances of infinite wavelength. To this end, we perform systematic experiments with inlet frequencies spanning the entire range of 0.167–1.5 Hz. Results of such experiments for channel width w=250 mm and two inclination angles, $\varphi=10°$ and 15°, are shown in Table I. Also shown in Table I is the critical Re predicted theoretically for each different frequency by a standard numerical solution of the Orr–Sommerfeld equation that governs the 2D linear stability problem.[22] It is noted that even the highest frequencies used become theoretically unstable at a Re that deviates less than 4% from the theoretical critical Re of infinite wavelength disturbances. Thus, these data confirm the lack of dependence on frequency in the low-frequency range used in the experiments and at the same time, their scatter serves as an indication of measurement precision. In particular, the standard deviation is about 3%–4% of the respective mean values, supporting an estimated experimental accuracy better than 5%.

B. Effect of channel width

The main finding of the present paper is that a restriction of the channel width strongly stabilizes film flow at small inclinations. The primary data supporting this conclusion are plotted in Figs. 7(a) and 7(b). Figure 7(a) shows the experimentally determined critical Re as a function of inclination angle and indicates that the deviation from the theoretical prediction, Eq. (1), grows with decreasing inclination. The same data are plotted in Fig. 7(b) using channel width as the dependent variable and the inclination as parameter. Here is becomes evident that the variation of critical Re with channel width is strong at small inclinations but becomes gradually insignificant beyond $\varphi=30°$. In other words, a channel 250 mm wide is narrow at $\varphi=5°$, but is equivalent to an infinitely wide channel at $\varphi=30°$.

Representative conditions are duplicated in the 3000 mm long facility and produce identical results within experimental accuracy. Most notably, experiments with the full channel width (450 mm) at inclination $\varphi=5°$ result in a threshold

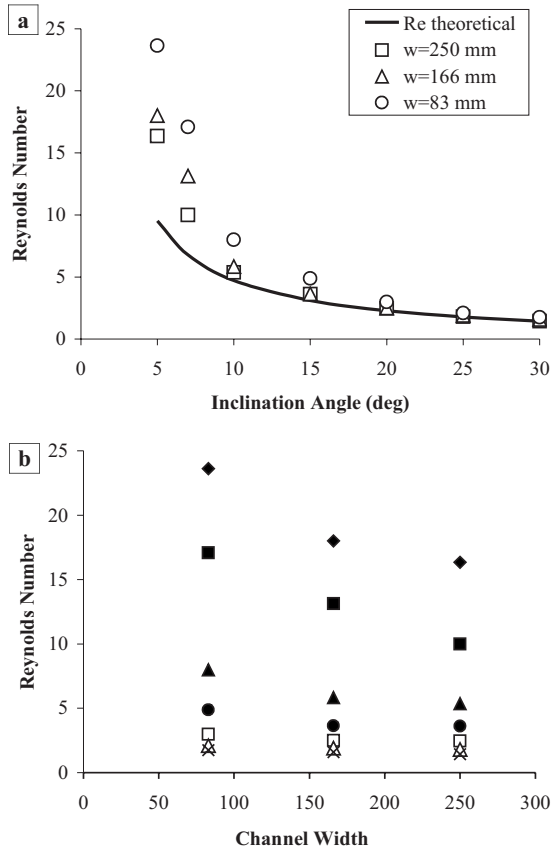

FIG. 7. The experimental critical Reynolds number as a function of (a) the inclination angle for three channel widths and (b) the channel width for inclination angles $\varphi=5°$ (♦), 7° (■), 10° (▲), 15° (●), 20° (□), 25° (△), and 30° (×).

value of Re=11.4, which is 20% above the classical prediction. This proves that the presently investigated effect extends at small inclinations to very wide channels.

Next, we attempt a rescaling of the stability results of Fig. 7(b) so that all data collapse on a single curve. Rescaling

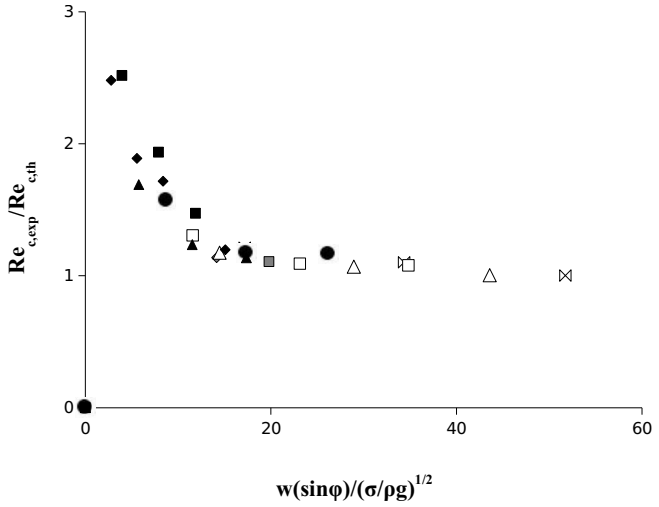

FIG. 8. The experimental critical Re, normalized with the theoretical value, as a function of dimensionless channel width. Symbols correspond to inclination angles $\varphi=5°$ (♦), 7° (■), 10° (▲), 15° (●), 20° (□), 25° (△), and 30° (×). Gray-filled symbols are for water-glycerol solutions saturated with butanol and inclination angles 5° and 7°, respectively.

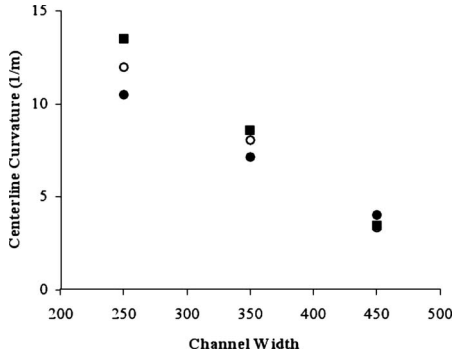

FIG. 9. The transverse curvature of the wave crestline at the channel centerplane, as a function of channel width. Data are for inclinations $\varphi=3°$ (●, Re=35), $\varphi=5°$ (○, Re=25), and $\varphi=10°$ (■, Re=12).

is straightforward for the *y*-axis and amounts to normalizing the experimental critical Re with the theoretical critical Re at the specific inclination. Thus, all measurements are compared with the wide-channel limit $\mathrm{Re}_{c,\mathrm{exp}}/\mathrm{Re}_{c,\mathrm{th}}=1$. Rescaling of the channel width is more puzzling and will be accomplished on a trial-and-error basis. More specifically, data indicate a strong effect of inclination angle but independence from liquid viscosity. Also, few experiments with significantly reduced surface tension (water-glycerol solution, saturated with butanol) show that surface tension is also relevant and may be taken into account by the streamwise capillary

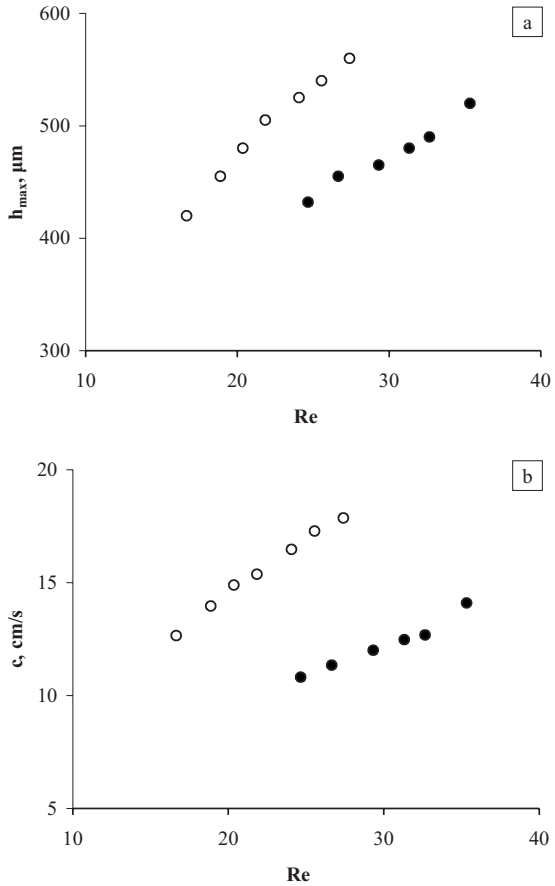

FIG. 10. The maximum film thickness (a) and the phase velocity (b) of the waves, as a function of Re for two channel widths, w=250 mm (●) and 450 mm (○) at an inclination of $\varphi=5°$.

length scale $L_s=(\sigma/\rho g \sin\theta)^{1/2}$. All these observations are summarized in Fig. 8, where the scaling eventually adopted for the x-axis is $w(\sin\theta)^{1/2}/L_s = w \sin\theta/(\sigma/\rho g)^{1/2}$. Though this choice appears to work well for the parameter range tested in the present paper, we cannot support it with a complete theoretical justification.

The scaling in Fig. 8 suggests that, unlike the classical prediction, the primary transition in channels of finite width may depend on surface tension. In particular, the higher the surface tension, the more significant the delay in the onset of traveling waves. Though these preliminary findings need to be thoroughly checked, they will be shown in Sec. IV to be reconciled with the expected effect of the additional capillary forces resulting from the curved crestline of traveling disturbances.

C. Properties of post-transition traveling waves

We have noted in the introduction that the channel sidewalls are generally considered responsible for the curved crestlines of fully developed traveling waves in the unstable regime. The present experimental evidence, about the effect of channel width on the transition threshold, indicates the sidewalls also modify the primary instability. A plausible conclusion is that the two phenomena are causally related, i.e., the crestline curvature, attained by initially 2D disturbances as they more downstream, leads to stronger attenuation and results in displacement of the transition to higher Re values.

In order to strengthen the above view, we provide some preliminary information on the characteristics of curved traveling waves observed in the unstable regime. (Detailed exposition of the properties of these nominally 2D waves will be the topic of a future paper). Thus, Figs. 9 and 10 present data of fully developed waves from the 3000 mm long facility and for channels 250, 350, and 450 mm wide.

Figure 9 displays representative results on the variation with channel width of the curvature of the wave crestline, as measured at the channel centerplane. The data are for inclinations $\varphi=3°$ (●, Re=35), $\varphi=5°$ (○, Re=25), and $\varphi=10°$ (■, Re=12). It is evident that the wave curvature depends strongly on channel width and varies inversely with it. Thus, disturbances in a narrow channel are subjected to stronger transverse capillary forces, an observation that is consistent with their delayed destabilization.

Figures 10(a) and 10(b) show, respectively, the maximum film thickness and the phase velocity of the waves, as a function of Re for two channel widths, w=250 mm (●) and 450 mm (○) at an inclination of $\varphi=5°$. It is readily observed that, at the same Re, waves in the narrower channel are shorter and slower. Again, a plausible explanation is that the waves are decelerated by the transverse capillary forces and as a result, the rate of work done by the perturbation shear stress decreases and the instability becomes weaker in narrower channels.

Finally, we comment briefly on the periodicity properties of post-threshold waves and their relation to the input forcing. To this end, we construct in Fig. 11 phase portraits of the time series in Fig. 3 (downstream point), following similar

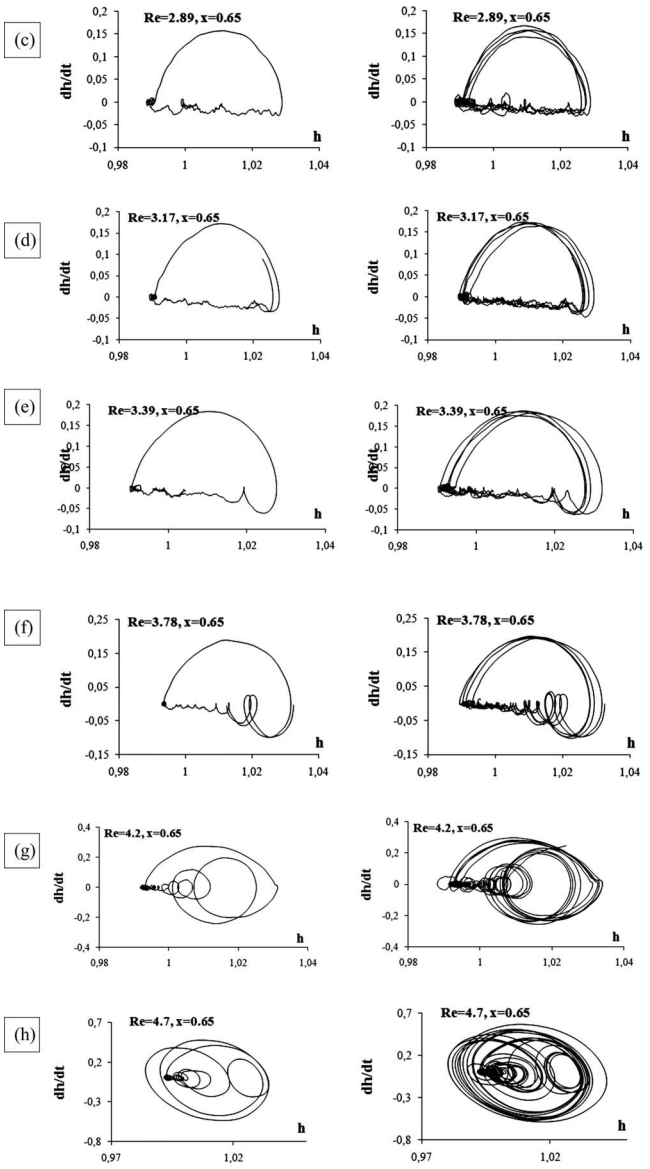

FIG. 11. Phase portraits of the last six time signals in Fig. 3. Left column is drawn for one period and right column for four periods of the inlet forcing.

TABLE I. The theoretical and the experimental critical Reynolds number as a function of frequency for channel width w=250 mm and inclination angles $\varphi=10°$ and 15°.

Frequency (Hz)	$\varphi=10°$		$\varphi=15°$	
	$Re_{c,th}$	$Re_{c,exp}$	$Re_{c,th}$	$Re_{c,exp}$
0.16	4.73	5.40	3.12	3.62
0.25	4.74	5.23	3.12	3.58
0.50	4.75	5.41	3.13	4.08
0.75	4.77	5.63	3.15	3.87
1.00	4.81	5.58	3.17	3.71
1.25	4.85	5.30	3.20	3.85
1.50	4.90	5.20	3.24	3.93
Mean		5.39		3.81
StDiv*100/Mean		3.07%		4.12%

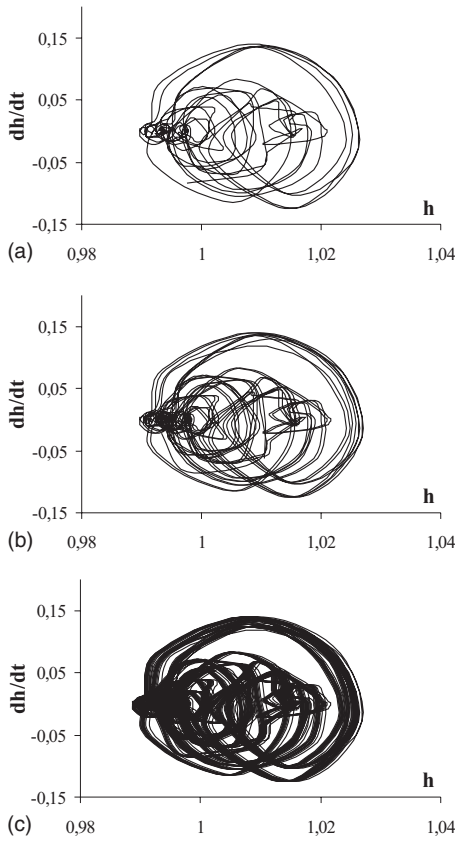

FIG. 12. Phase portraits of a wave profile with large number of secondary crests (φ=15°, w=166 mm, Re=4.78, and f=0.25 Hz), constructed from time signals with duration (a) four, (b) eight, and (c) 160 periods of the inlet forcing.

approaches in the literature.[23,24] The left column represents phase portraits for one period of the inlet forcing and the right column for four periods. In both columns, we plot results for the six larger Re's in Fig. 3 and to facilitate comparisons between signals and portraits, we retain the same numbering (c)–(h).

It is noted that the forcing frequency is always present and is still dominant beyond transition [Figs. 11(c)–11(f)]. The curls that gradually appear at the right end of the main cycle correspond to the secondary crests developing on top of the main hump. With further increase in Re, these secondary crests gradually exert stronger influence and eventually dominate the phase portrait [Figs. 11(g) and 11(h)]. However, the phenomenon is still considered as periodic with slight variations between cycles being understood as the result of experimental imperfection in the realization of consecutive periods of forcing.

In order to further support this last point, we present in Fig. 12, phase portraits for experimental conditions that result in a large number of secondary crests. Figure 12(a) alone, which is constructed from a time signal with duration four periods of the inlet forcing, would leave reasonable doubt about the periodicity of the phenomenon. However, Fig. 12(b) (eight periods) and most important Fig. 12(c) (160 periods) confirm that this complex signal is still periodic. We conclude that periodicity is retained for a range of Re beyond the primary instability. The transition to a nonperiodic free surface, which is expected to occur at higher Re is beyond the scope of the present work.

IV. CONCLUDING REMARKS

This work investigated the effect of channel width on the primary instability of inclined film flow. To this end, a procedure was developed, based on conductivity probes, which permitted accurate determination of the transition with modest effort. The data showed that liquid films at small and intermediate inclination angles are significantly more stable than previously believed and the deviation from the classical prediction scales inversely with the product of channel width and sine of inclination angle. This unexpected finding was attributed to the influence of sidewalls on traveling disturbances, and more specifically to the downstream development of a curved crestline. Preliminary results on the properties of post-transition traveling waves and in particular their variation with channel width were used to support this view.

The present findings motivate a detailed study of the characteristics of the traveling waves that appear beyond the bifurcation threshold. Of particular interest are the effect of channel width and the deviations from the theoretically expected 2D behavior. In this respect, the conditions close to the wall need to be carefully considered, as the additional viscous and capillary forces (due, respectively, to the boundary layer and change in curvature close to the sides) are expected to strongly influence the local wave characteristics.

Preliminary findings (and also a careful examination of Fig. 1) indicate that the streamwise steepness of these waves varies symmetrically along the crestline with maximum at the centerplane and decreasing height of the main hump (and increasing wavelength of the precursor ripples) toward the sidewalls. Thus, these nominally 2D waves have a qualitative similarity to the horseshoe waves that appear either naturally at much higher Re (Ref. 25) or artificially by localized addition of liquid mass.[26–28] Of course, the two kinds of waves differ in length scale with the former scaling according to the channel width and the latter being much smaller. It is envisioned that this similarity in shape and difference in scale may permit a unified treatment of the nominally 2D and the 3D flow regimes, and may offer an interpretation of the 2D-to-3D transition in terms of a gradual reduction of the scale of the largest stable curved wave.

ACKNOWLEDGMENTS

The present work was partly supported by the EU under the Marie-Curie Initial Training Network "Multiflow" (GA Grant No. 214919-2). An illuminating discussion of bifurcation phenomena with Professor Alex Oron is gratefully acknowledged.

[1] R. W. Chin, F. H. Abernathy, and J. R. Bertschy, "Gravity and shear wave stability of free surface flows. Part 1. Numerical calculations," J. Fluid Mech. **168**, 501 (1986).
[2] A. Oron, S. H. Davis, and S. G. Bankof, "Long-scale evolution of thin liquid films," Rev. Mod. Phys. **69**, 931 (1997).
[3] R. E. Kelly, D. A. Goussis, S. P. Lin, and F. K. Hsu, "The mechanism for

surface wave instability in film flow down an inclined plane," Phys. Fluids A **1**, 819 (1989).
[4]M. K. Smith, "The mechanism for the long-wave instability in thin liquid films," J. Fluid Mech. **217**, 469 (1990).
[5]T. B. Benjamin, "Wave formation in laminar flow down an inclined plane," J. Fluid Mech. **2**, 554 (1957).
[6]C.-S. Yih, "Stability of liquid flow down an inclined plane," Phys. Fluids **6**, 321 (1963).
[7]H.-C. Chang and E. A. Demekhin, *Complex Wave Dynamics on Thin Films* (Elsevier, Amsterdam, 2002).
[8]E. A. Demekhin, E. N. Kalaidin, S. Kalliadasis, and S. Yu. Vlaskin, "Three-dimensional localized coherent structures of surface turbulence. I. Scenarios of two-dimensional-three-dimensional transition," Phys. Fluids **19**, 114103 (2007).
[9]J. Liu, J. D. Paul, and J. P. Gollub, "Measurements of the primary instabilities of film flow," J. Fluid Mech. **250**, 69 (1993).
[10]G. D. Fulford, "The flow of liquids in thin films," Adv. Chem. Eng. **5**, 151 (1964).
[11]M. Scholle and N. Aksel, "An exact solution of visco-capillary flow in an inclined channel," ZAMP **52**, 749 (2001).
[12]C. Pozrikidis, *Introduction to Theoretical and Computational Fluid Dynamics* (Oxford, New York, 1997).
[13]S. V. Alekseenko, V. E. Nakoryakov, and B. G. Pokusaev, *Wave Flow of Liquid Films* (Begell House, New York, 1994).
[14]J. Liu and J. P. Gollub, "Solitary wave dynamics of film flows," Phys. Fluids **6**, 1702 (1994).
[15]M. Vlachogiannis and V. Bontozoglou, "Observations of solitary wave dynamics of film flows," J. Fluid Mech. **435**, 191 (2001).
[16]B. Ramaswamy, S. Chippada, and S. W. Joo, "A full-scale numerical study of interfacial instabilities in thin-film flows," J. Fluid Mech. **325**, 163 (1996).
[17]N. Malamataris, M. Vlachogiannis, and V. Bontozoglou, "Solitary waves on inclined films: Flow structure and binary interactions," Phys. Fluids **14**, 1082 (2002).
[18]D. Gao, N. B. Morley, and V. Dhir, "Numerical simulation of wavy falling film flow using VOF method," J. Comput. Phys. **192**, 624 (2003).
[19]T. Nosoko and A. Miyara, "The evolution and subsequent dynamics of waves on a vertically falling liquid film," Phys. Fluids **16**, 1118 (2004).
[20]B. Scheid, C. Ruyer-Quil, and P. Manneville, "Wave patterns in film flows: Modeling and three-dimensional waves," J. Fluid Mech. **562**, 183 (2006).
[21]A. Wierschem, C. Lepski, and N. Aksel, "Effect of long undulated bottoms on thin gravity-driven films," Acta Mech. **179**, 41 (2005).
[22]P. J. Schmid and D. S. Henningson, *Stability and Transition in Shear Flows* (Springer-Verlag, Berlin, 2001).
[23]O. Gottlieb and A. Oron, "Stability and bifurcations of parametrically excited thin liquid films," Int. J. Bifurcation Chaos Appl. Sci. Eng. **14**, 4117 (2004).
[24]B. Uma and R. Usha, "A thin conducting viscous film on an inclined plane in the presence of a uniform normal electric field: Bifurcation scenarios," Phys. Fluids **20**, 032102 (2008).
[25]C. D. Park and T. Nosoko, "Three-dimensional wave dynamics on a falling film and associated mass transfer," AIChE J. **49**, 2715 (2003).
[26]S. V. Alekseenko, V. A. Antipin, V. V. Guzanov, S. M. Kharlamov, and D. M. Markovich, "Three dimensional solitary waves on falling liquid film at low Reynolds numbers," Phys. Fluids **17**, 121704 (2005).
[27]E. A. Demekhin, E. N. Kalaidin, S. Kalliadasis, and S. Yu. Vlaskin, "Three-dimensional localized coherent structures of surface turbulence. II. Λ solitons," Phys. Fluids **19**, 114104 (2008).
[28]C. E. Meza and V. Balakotaiah, "Modeling and experimental studies of large amplitude waves on vertically falling films," Chem. Eng. Sci. **63**, 4704 (2008).